Inorganic Chemistry

Article

pubs.acs.org/IC

Factors Affecting Hydrogen-Tunneling Contribution in Hydroxylation Reactions Promoted by Oxoiron(IV) Porphyrin π-Cation Radical Complexes

Zhiqi Cong,[‡] Haruki Kinemuchi,[†] Takuya Kurahashi,[‡] and Hiroshi Fujii*[,‡,†]

[†]Department of Chemistry, Biology and Environmental Science, Faculty of Science, Nara Women's University, Kitauoyanishi, Nara 830-8506, Japan

[‡]Institute for Molecular Science, National Institutes of Natural Sciences, Myodaiji, Okazaki 444-8787, Japan

Supporting Information

ABSTRACT: Hydrogen atom transfer with a tunneling effect (H-tunneling) has been proposed to be involved in aliphatic hydroxylation reactions catalyzed by cytochrome P450 and synthetic heme complexes as a result of the observation of large hydrogen/deuterium kinetic isotope effects (KIEs). In the present work, we investigate the factors controlling the H-tunneling contribution to the H-transfer process in hydroxylation reaction by examining the kinetics of hydroxylation reactions at the benzylic positions of xanthene and 1,2,3,4-tetrahydronaphthalene by oxoiron(IV) 5,10,15,20-tetramesitylporphyrin π-cation radical complexes ((TMP$^{+\bullet}$)Fe^{IV}O(L)) under single-turnover conditions. The Arrhenius plots for these hydroxylation reactions of H-isotopomers have upwardly concave profiles. The Arrhenius plots of D-isotopomers, clear isosbestic points, and product analysis rule out the participation of thermally dependent other reaction processes in the concave profiles. These results provide evidence for the involvement of H-tunneling in the rate-limiting H-transfer process. These profiles are simulated using an equation derived from Bell's tunneling model. The temperature dependence of the KIE values (k_H/k_D) determined for these reactions indicates that the KIE value increases as the reaction temperature becomes lower, the bond dissociation energy (BDE) of the C−H bond of a substrate becomes higher, and the reactivity of (TMP$^{+\bullet}$)Fe^{IV}O(L) decreases. In addition, we found correlation of the slope of the $\ln(k_H/k_D) - 1/T$ plot and the bond strengths of the Fe═O bond of (TMP$^{+\bullet}$)Fe^{IV}O(L) estimated from resonance Raman spectroscopy. These observations indicate that these factors modulate the extent of the H-tunneling contribution by modulating the ratio of the height and thickness of the reaction barrier.

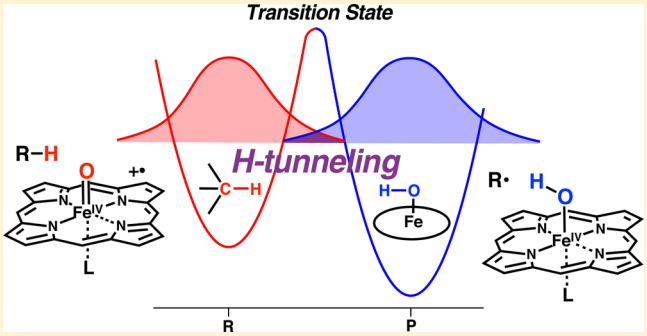

INTRODUCTION

Hydroxylation reactions of alkanes have received significant attention for decades due to their importance in biological and chemical reactions.[1−17] Cytochrome P450 catalyzes various hydroxylation reactions under mild conditions in the degradation of many xenobiotics and the synthesis of physiologically important compounds such as steroid hormones.[1,3,4,10,11] Since Groves et al. reported the first example of alkane hydroxylation reactions with chloro iron(III) *meso*-tetraphenylporphyrin (TPP) complex and iodosylbenzene as a terminal oxidant,[12] many synthetic heme catalysts for alkane hydroxylation reactions have also been prepared.[3,6,9,13−17] In these reactions, oxoiron(IV) porphyrin π-cation radical species (which are collectively known as compound I) have been accepted as the key reactive intermediates responsible for the hydroxylation reactions.[18−23]

The generally accepted mechanism for alkane hydroxylations catalyzed by cytochrome P450 and synthetic heme catalysts is the "oxygen rebound" mechanism (Scheme 1) originally proposed by Groves et al.[24] The oxoiron(IV) porphyrin π-cation radical species initially abstracts a hydrogen atom from a C−H bond of an alkane substrate to produce an alkane radical and an iron(IV)-hydroxide intermediate (or iron(III)-hydroxide porphyrin π-cation radical intermediate). The alkane radical then rebounds with the hydroxide ligand of the intermediate to form an iron(III) porphyrin and alcohol. In this mechanism, it has been proposed that the initial hydrogen atom transfer process from the alkane to the oxo ligand is the rate-limiting step of the hydroxylation reaction. Therefore, it is essential to understand the process of hydrogen atom transfer in order to understand the hydroxylation reaction.

Scheme 1

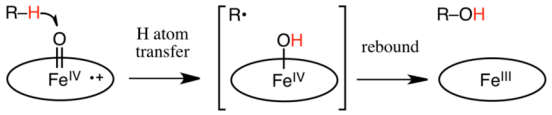

Received: July 18, 2014
Published: September 15, 2014

Among the most intriguing observations made during the hydrogen atom transfer processes are the unusually large hydrogen(H)/deuterium(D) primary kinetic isotope effects (KIEs).[25−42] Such large KIE values have been ascribed to a significant contribution of quantum-mechanical tunneling of hydrogen or proton (H-tunneling) in the rate-limiting hydrogen atom transfer process.[43−61] H-tunneling in the hydrogen atom transfer process from a substrate to an oxoiron species is described in Scheme 2. The classical transition state

Scheme 2

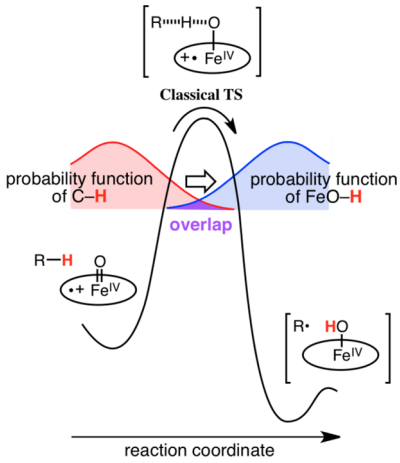

theory predicts that a hydrogen atom can be transferred from the substrate to the oxo ligand by surmounting a reaction barrier only if its energy is greater than the barrier height. However, the H-tunneling effect predicts that a hydrogen atom with even less energy may also be transferred by overlapping probability functions of reactant and product states. Several consequences for the participation of H-tunneling in the hydrogen atom transfer reaction are (1) an anomalously large KIE value, $k_H/k_D > 10$ at 25 °C for C−H bond, (2) a greater difference between the observed activation energies for hydrogen- and deuterium-isotopomers, $E(H)$ and $E(D)$, than that expected from zero-point energy, $E(D) - E(H) > 5.66$ kJ mol^{-1} for C−H bond, and (3) an unusually low value of the ratio of experimental Arrhenius prefactors for H- and D-isotopomers: $A^H_{obs}/A^D_{obs} < 0.7$.[43−61] In an extreme case, the profile of the Arrhenius plot has an upward concave shape instead of linear behavior.

There have been many reports that suggest the participation of the H-tunneling process in hydroxylation reactions. For example, the ambient temperature KIE values (k_H/k_D) were found to be more than ∼7: 7−12 for aliphatic hydroxylations catalyzed by cytochrome P450 and 7−22 for those by synthetic heme complexes.[25−32] Large KIE values have also been reported for nonheme enzymes and their model complexes.[33−42] Recently, larger KIE values (∼28 at 23 °C and ∼360 at −30 °C) have been reported for a benzyl alcohol oxidation reaction catalyzed by an oxoiron(IV) 5,10,15,20-tetramesitylporphyrin (TMP) π-cation radical complex, (TMP$^{+\bullet}$)Fe^{IV}O(L).[32] The Arrhenius plot for the benzyl alcohol oxidation reaction showed linear behavior from 23 to −30 °C, but it showed a large difference in the activation energy and the Arrhenius pre-exponential factor between benzyl alcohol and benzyl alcohol-d_7. These data were simulated with Bell's tunneling model. So far, there is no report of nonlinear behavior of the Arrhenius plot for hydroxylation reaction of C−H bond by high-valent metal-oxo speices.

In the present work, to study the factors affecting the H-tunneling process, we performed a kinetic study of hydroxylation reactions at the benzylic positions of xanthene and 1,2,3,4-tetrahydronaphthalene (tetralin) promoted by (TMP$^{+\bullet}$)Fe^{IV}O(L) under single-turnover conditions in dichloromethane at low-temperature (Figure 1). The effect of

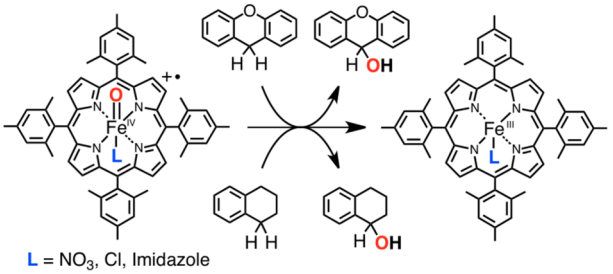

Figure 1. Hydroxylation reactions at the benzylic positions of xanthene and tetralin catalyzed by (TMP$^{+\bullet}$)Fe^{IV}O(L).

reactivity of (TMP$^{+\bullet}$)Fe^{IV}O(L) on the H-tunneling process is studied by changing the axial ligand (L): nitrate, (TMP$^{+\bullet}$)-Fe^{IV}O(NO$_3$); chloride, (TMP$^{+\bullet}$)Fe^{IV}O(Cl), and imidazole, [(TMP$^{+\bullet}$)Fe^{IV}O(Im)](NO$_3$).[62] The effect of the bond dissociation energy (BDE) of the substrate C−H bond is studied using xanthene (BDE: 75−76 kcal mol^{-1}) and tetralin (BDE: 82−83 kcal mol^{-1}) as substrates.[63] The Arrhenius plots for these hydroxylation reactions show nonlinear Arrhenius behavior, which provides strong evidence for the participation of H-tunneling in the rate-limiting hydrogen transfer process. The results presented here provide evidence that the contribution of the H-tunneling is controlled by the reaction temperature, the BDE of the C−H bond of the substrate, the reactivity of (TMP$^{+\bullet}$)Fe^{IV}O(L), and probably the Fe═O bond strength of (TMP$^{+\bullet}$)Fe^{IV}O(L).

RESULTS

Reaction of (TMP$^{+\bullet}$)Fe^{IV}O(NO$_3$) with Xanthene. (TMP$^{+\bullet}$)Fe^{IV}O(NO$_3$) was prepared by oxidation of (TMP)-Fe^{III}(NO$_3$) with ozone in dichloromethane at low-temperature.[62] Since excess ozone gas and formed oxygen gas from the oxidation can be removed from reaction solution by argon bubbling, the ozone oxidation is cleaner than the other chemical oxidations, in which excess oxidants and a byproduct formed from the oxidants are usually present. Figure 2 shows the absorption spectral change occurring during the reaction of (TMP$^{+\bullet}$)Fe^{IV}O(NO$_3$) with 20 equiv of xanthene at −50 °C. The absorption spectrum of (TMP$^{+\bullet}$)Fe^{IV}O(NO$_3$), which shows strong absorption at 667 nm, changes, with clear isosbestic points, to that of (TMP)Fe^{III}(NO$_3$), which has absorption peaks at 512, 583, and 693 nm. The same absorption spectral change was observed in the temperature range from −20 to −95 °C. The presence of the clear isosbestic points indicates that a simple oxidation reaction of xanthene occurs in the present conditions. Analysis of the reaction product by ^{1}H NMR spectroscopy indicates formation of xanthydrol as a major product (Table 1 and Supporting Information Figure S1). In addition, a small amount of xanthone, which is an overoxidation product of xanthene, was formed. However, no other aromatic hydroxylation products were detected. This result is similar to the result obtained in a

dx.doi.org/10.1021/ic501737j | Inorg. Chem. 2014, 53, 10632−10641

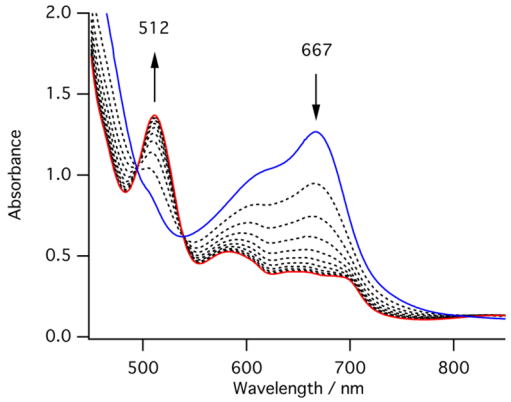

Figure 2. UV−vis absorption spectral change for the reaction of $(TMP^{+\bullet})Fe^{IV}(O)(NO_3)$ (1.0×10^{-4} M in optical path length 1 cm cell) and xanthene (2.0×10^{-3} M) in dichloromethane at −50 °C: blue solid line, $(TMP^{+\bullet})Fe^{IV}(O)(NO_3)$; black dotted line, every 200 s after addition of xanthene; red solid line, after 2000 s.

Table 1. Products and Their Yields for the Reaction of $(TMP^{+\bullet})Fe^{IV}O(L)$ with Xanthene[a]

		product and yield (%)	
complex	T (°C)	xanthydrol	xanthone
$(TMP^{+\bullet})Fe^{IV}O(NO_3)$	−30 °C	75	10
	−90 °C	79	13
$(TMP^{+\bullet})Fe^{IV}O(Cl)$	−50 °C	84	4
	−90 °C	86	6
$[(TMP^{+\bullet})Fe^{IV}O(Im)](NO_3)$	−60 °C	97	not detected
	−90 °C	95	not detected

[a]Experiment conditions were shown in the Experimental Section. The yields are averages of two or three independent experiments.

previous report.[64] The yields of xanthene and xanthone were not changed at −30 and −90 °C. These results indicate that the observed absorption spectral change results from the benzylic hydroxylation of xanthene.

To study the involvement of the H-tunneling, we conducted a kinetic study of the xanthene hydroxylation reaction in dichloromethane over the temperature range −20 to −95 °C. The time courses of the changes in absorbance at 667 nm were found to follow the first-order kinetics in the presence of excess (>10-fold) xanthene (Supporting Information Figure S2 and Table S1). The estimated reaction rate constant, k_{obs}, is linearly correlated with the concentration of xanthene (Supporting Information Figure S3). This is used to determine the second-order reaction rate constant. The estimated second-order rate constants, k_2's, are listed in Table 2 and plotted in the Arrhenius plot (Figure 3). The plot cannot be simulated with a line as expected from the Arrhenius equation, but has an upward concave profile. The deviation from the linear behavior predicted by the Arrhenius equation suggests the involvement of other reaction processes, such as the H-tunneling process.

To confirm the involvement of the H-tunneling process, we conducted kinetic studies of the hydroxylation reaction of $(TMP^{+\bullet})Fe^{IV}O(NO_3)$ with deuterium-labeled xanthene-d_2, in which two hydrogen atoms at the 9 position are replaced with deuterium atoms, over the temperature range from −70 to −20 °C (Supporting Information Figures S4 and S5 and Table S2). Reliable reaction rate constants could not be obtained outside this temperature range because the reaction is too slow at temperature below −70 °C due to limited substrate solubility

Table 2. Second-Order Reaction Rate Constants (k_2) for the Reaction of $(TMP^{+\bullet})Fe^{IV}O(NO_3)$ with Xanthene and Xanthene-d_2

	$k_2/M^{-1}\ s^{-1}$		
T/°C	xanthene	xanthene-d_2	KIE[a]
−20	3.93 ± 0.02	(2.34 ± 0.03) × 10^{-1}	16.8 (17.4)
−30	2.69 ± 0.08	(1.28 ± 0.05) × 10^{-1}	21.0 (21.9)
−40	1.62 ± 0.07	(6.04 ± 0.25) × 10^{-2}	26.8 (28.3)
−50	(9.64 ± 0.20) × 10^{-1}	(2.82 ± 0.05) × 10^{-2}	34.2 (36.6)
−60	(5.91 ± 0.10) × 10^{-1}	(1.19 ± 0.06) × 10^{-2}	49.7 (55.1)
−70	(3.45 ± 0.07) × 10^{-1}	(5.45 ± 0.03) × 10^{-3}	63.3 (72.5)
−80	(2.08 ± 0.04) × 10^{-1}		
−90	(1.27 ± 0.04) × 10^{-1}		
−95	(8.92 ± 0.20) × 10^{-2}		

[a]The numbers in parentheses are KIE values obtained after an isotope purity correction with isotope purity 99.8% for xanthene-d_2.

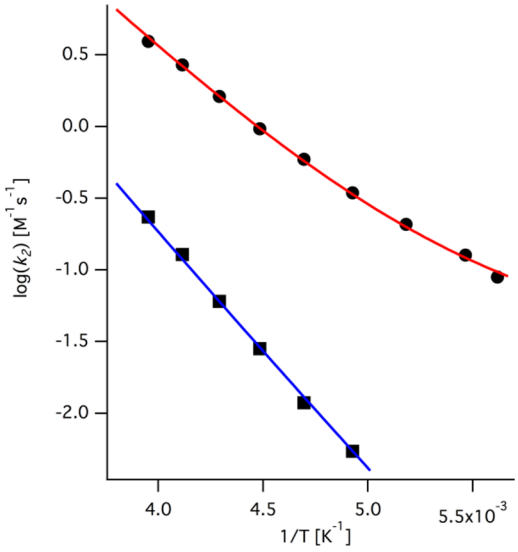

Figure 3. Arrhenius plots using second-order rate constants listed in Table 2 for the hydroxylation reactions of $(TMP^{+\bullet})Fe^{IV}O(NO_3)$ with xanthene (●) and xanthene-d_2 (■). The lines (red line for xanthene and blue line for xanthene-d_2) are results of least-squares fits with Bell's tunneling model, eq1. The estimated parameters are listed in Table 3.

and because the decomposition of $(TMP^{+\bullet})Fe^{IV}O(NO_3)$ is too fast at temperature above −20 °C. The estimated second-order reaction rate constants are summarized in Table 2 and plotted in the Arrhenius plot (Figure 3). The Arrhenius plot for xanthene-d_2 is almost linear. This clearly rules out the participation of thermally dependent other reaction processes, such as two reactive species suggested by Shiak et al., in the observed upwardly concaved profile.[65] The Arrhenius prefactor ($\log A^{H}_{obs} = 4.4$) estimated using a linear function for xanthene is smaller than that ($\log A^{D}_{obs} = 6.1$) for xanthene-d_2, $A^{H}_{obs}/A^{D}_{obs} = 0.02$ (Supporting Information Figure S6). This is consistent with a significant contribution of the H-tunneling process.

To further confirm the nonlinear Arrhenius behaivior, we analyzed the Arrhenius plot using Bell's tunneling model,[43,52a] in which the reaction potential curve is assumed to be a symmetrical truncated parabola and the reaction proceeds via both the classical transition state pathway and the H-tunneling pathway. This model is classical and too simple to evaluate the

dx.doi.org/10.1021/ic501737j | Inorg. Chem. 2014, 53, 10632−10641

Table 3. Parameters Estimated from Least-Square Fits of Arrhenius Plots with Bell's Tunneling Model

substrate	iron porphyrin	$\nu_{Fe=O}$/cm^{-1}	log A/M^{-1} s^{-1}	a/Å	E(H)/kJ mol^{-1}	E(D)/kJmol^{-1}
xanthene (75.5)[a]	(TMP$^{+\bullet}$)Fe^{IV}O(NO$_3$)	821[c]	6.2 ± 0.1	0.504 ± 0.003	29.8 ± 0.1	34.9 ± 0.1
					(33.8 ± 1.0)[b]	(38.6 ± 0.9)[b]
	(TMP$^{+\bullet}$)Fe^{IV}O(Cl)	801[c]	6.2 ± 0.1	0.519 ± 0.006	24.6 ± 0.1	29.1 ± 0.1
					(20.2 ± 1.1)[b]	(25.1 ± 1.0)[b]
	[(TMP$^{+\bullet}$)Fe^{IV}O(Im)]NO$_3$	812[d]	6.9 ± 0.2	0.504 ± 0.004	28.0 ± 0.1	31.5 ± 0.1
					(28.7 ± 0.6)[b]	(32.1 ± 0.5)[b]
tetraline (82.5)[a]	(TMP$^{+\bullet}$)Fe^{IV}O(Cl)	801[c]	5.8 ± 0.1	0.566 ± 0.006	29.9 ± 0.1	35.1 ± 0.1
					(41.7 ± 1.6)[b]	(46.9 ± 1.4)[b]

[a]The numbers in the parentheses are the bond dissociation energy (kcal mol^{-1}) of the C–H bonds at the benzyl positions.[63] [b]The numbers in the parentheses are E(H) and E(D) values estimated from least-squares fits of Figure 6. [c]Reference 66. [d]Reference 67.

parameters for potential energy surface, in contrast to recently proposed models based on first principles.[57−61] However, this is convenient and sufficient just to show nonlinear Arrhenius behavior including the H-tunneling. In Bell's tunneling model, the temperature dependence of the reaction rate constant (k) can be described as

$$k = A\frac{(\beta e^{-\alpha} - \alpha e^{-\beta})}{\beta - \alpha} \quad (1)$$

where $\alpha = ((E)/(k_B T))$ and $\beta = ((2\pi^2 a(2mE)^{1/2})/(h))$. In this equation, A is the Arrhenius prefactor, E is the height of the reaction barrier, k_B is the Boltzmann constant, T is reaction temperature (K), h is the Planck constant, a is half of the width at the bottom of the parabolic barrier, and m is the mass of a hydrogen atom or a deuterium atom. The Arrhenius plots for the reactions of (TMP$^{+\bullet}$)Fe^{IV}O(NO$_3$) with xanthene and xanthene-d_2 were simulated with eq 1, and the results are shown with red and blue lines, respectively, in Figure 3. The estimated parameters from the simulations are summarized in Table 3. The E(D) − E(H) value (5.1 kJ/mol) is within the range of a semiclassical transition state model, in which less than 5.66 kJ/mol is expected with allowance for bending vibrations. The simulation line expected from eq 1 fits the data better than that from the Arrhenius linear equation. This is confirmed more clearly by the T log k–T plot (Supporting Information Figure S7).

Reaction of (TMP$^{+\bullet}$)Fe^{IV}O(L) with Xanthene. To study the effect of the reactivity of an oxoiron(IV) porphyrin π-cation radical complex on the H-tunneling process in the hydroxylation reaction, we conducted kinetic studies of the hydroxylation reaction of (TMP$^{+\bullet}$)Fe^{IV}O(Cl) and [(TMP$^{+\bullet}$)Fe^{IV}O(Im)](NO$_3$) with xanthene in dichloromethane. Previously, we showed that reactivity for epoxidation of cyclooctene increases according to the following order: (TMP$^{+\bullet}$)Fe^{IV}O(NO$_3$) < (TMP$^{+\bullet}$)Fe^{IV}O(Cl) < [(TMP$^{+\bullet}$)Fe^{IV}O(Im)](NO$_3$).[62] With addition of xanthene, the absorption spectra of (TMP$^{+\bullet}$)Fe^{IV}O(Cl) and [(TMP$^{+\bullet}$)Fe^{IV}O(Im)](NO$_3$) change to those of iron(III) porphyrin complexes with clear isosbestic points (Supporting Information Figure S8). The product analysis indicates the formation of xanthydrol in 84% yield at −50 °C and in 97% yield at −60 °C from the reactions of (TMP$^{+\bullet}$)Fe^{IV}O(Cl) and [(TMP$^{+\bullet}$)Fe^{IV}O(Im)](NO$_3$), respectively (Table 1 and Supporting Information Figure S1). The similar yields were also obtained at −90 °C, suggesting no change of the reaction mechanism even at low-temperature (Table 1).

The second-order reaction rate constants (k_2) of (TMP$^{+\bullet}$)Fe^{IV}O(Cl) and [(TMP$^{+\bullet}$)Fe^{IV}O(Im)](NO$_3$) with xanthene were estimated from the dependence of the reaction rate constant (k_{obs}) on the concentration of xanthene and xanthene-d_2 (Tables 4 and 5, and Supporting Information Figures S9–S16 and Tables S3–S6), and the results are plotted in the Arrhenius plot (Figure 4). It is interesting to note that k_2 for the xanthene hydroxylation reaction increases according to the order (TMP$^{+\bullet}$)Fe^{IV}O(NO$_3$) < (TMP$^{+\bullet}$)Fe^{IV}O(Cl) < [(TMP$^{+\bullet}$)Fe^{IV}O(Im)](NO$_3$), which is the same as that for an cyclooctene epoxidation reaction.[62] The Arrhenius plots for the reactions of (TMP$^{+\bullet}$)Fe^{IV}O(Cl) and [(TMP$^{+\bullet}$)Fe^{IV}O(Im)](NO$_3$) with xanthene and xanthene-d_2 seem to be linear, but very slight deviations from linear lines can be detected for xanthene. The Arrhenius prefactors (log A^H_{obs} = 5.2 and 5.0) estimated with a linear function for (TMP$^{+\bullet}$)Fe^{IV}O(Cl) and [(TMP$^{+\bullet}$)Fe^{IV}O(Im)](NO$_3$) are smaller than those (log A^D_{obs} = 5.7 and 6.5) with xanthene-d_2, and, thus, A^H_{obs}/A^D_{obs} = 0.32 and 0.03, respectively (Supporting Information Figure S6). The Arrhenius plots can be simulated well with Bell's tunneling

Table 4. Second-Order Reaction Rate Constants for the Reaction of (TMP$^{+\bullet}$)Fe^{IV}O(Cl) with Xanthene and Xanthene-d_2

	k_2/M^{-1} s^{-1}		
T/°C	xanthene	xanthene-d_2	KIE[a]
−40	17.75 ± 0.25	(9.90 ± 0.14) × 10^{-1}	17.6 (18.5)
−50	10.31 ± 0.41	(5.16 ± 0.38) × 10^{-1}	20.0 (20.8)
−60	6.20 ± 0.22	(2.56 ± 0.07) × 10^{-1}	23.8 (25.0)
−70	3.85 ± 0.17	(1.28 ± 0.06) × 10^{-1}	28.0 (29.6)
−80	2.25 ± 0.05	(6.14 ± 0.06) × 10^{-2}	34.0 (36.4)
−90	1.29 ± 0.02	(2.72 ± 0.07) × 10^{-2}	45.9 (50.4)
−95	(9.92 ± 0.15) × 10^{-1}		

[a]The numbers in parentheses are KIE values obtained after isotope purity correction with isotope purity 99.8% for xanthene-d_2.

Table 5. Second-Order Reaction Rate Constants for the Reaction of [(TMP$^{+\bullet}$)Fe^{IV}O(Im)](NO$_3$) with Xanthene and Xanthene-d_2

	k_2/M^{-1} s^{-1}		
T/°C	xanthene	xanthene-d_2	KIE[a]
−50	11.59 ± 0.01	(8.97 ± 0.27) × 10^{-1}	12.9 (13.2)
−60	6.41 ± 0.27	(3.86 ± 0.01) × 10^{-1}	16.6 (17.1)
−70	4.04 ± 0.06	(1.77 ± 0.06) × 10^{-1}	22.9 (23.9)
−80	2.44 ± 0.08	(8.10 ± 0.25) × 10^{-2}	30.1 (32.0)
−90	1.44 ± 0.06	(3.16 ± 0.20) × 10^{-2}	45.6 (50.1)
−95	1.12 ± 0.01		

[a]The numbers in parentheses are KIE values obtained after isotope purity correction with isotope purity 99.8% for xanthene-d_2.

dx.doi.org/10.1021/ic501737j | Inorg. Chem. 2014, 53, 10632−10641

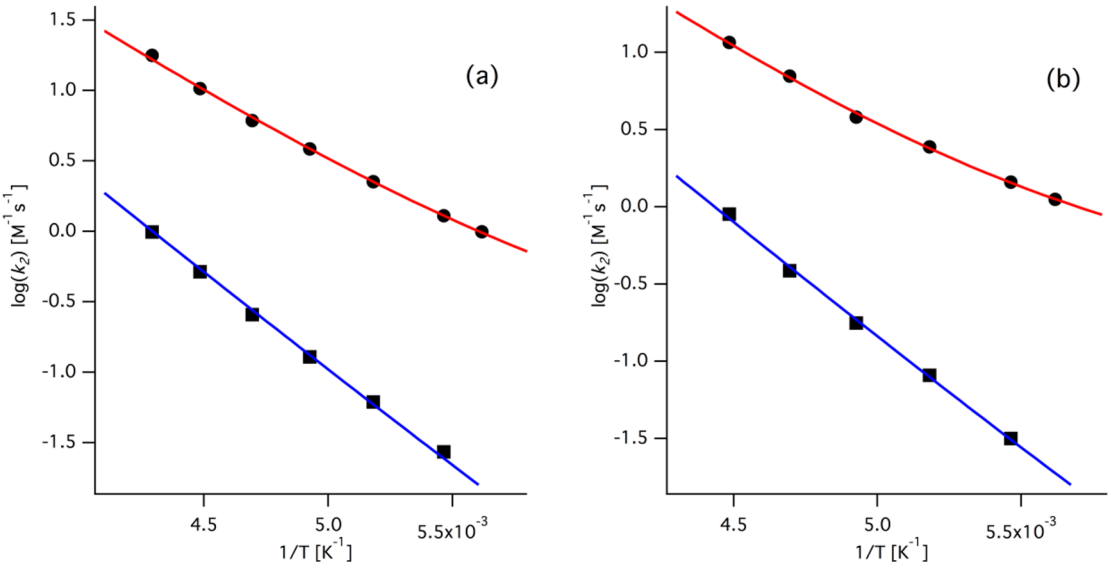

Figure 4. Arrhenius plots using the second-order rate constants listed in Tables 4 and 5 for the hydroxylation reactions of (a) $(TMP^{+\bullet})Fe^{IV}O(Cl)$ and (b) $[(TMP^{+\bullet})Fe^{IV}O(Im)](NO_3)$ with xanthene (●) and xanthene-d_2 (■). Solid lines (red line for xanthene and blue line for xanthene-d_2) are results obtained for the least-squares fits with Bell's tunneling model, eq 1. The estimated parameters are listed in Table 3.

model (eq 1) better than the Arrhenius linear function (Figure 4 and Supporting Information Figure S6). The estimated parameters are listed in Table 3. All of these results indicate significant contribution of the H-tunneling processes in these hydroxylation reactions of $(TMP^{+\bullet})Fe^{IV}O(Cl)$ and $[(TMP^{+\bullet})Fe^{IV}O(Im)](NO_3)$.

Reaction of $(TMP^{+\bullet})Fe^{IV}O(Cl)$ with Tetralin. To study the effect of the C−H bond dissociation energy on the H-tunneling process in a hydroxylation reaction, we conducted kinetic studies of the hydroxylation reaction of $(TMP^{+\bullet})Fe^{IV}O(Cl)$ with tetralin, which has higher C−H bond dissociation energy of the benzyl moiety than xanthene (Table 3). We examined the reaction of $(TMP^{+\bullet})Fe^{IV}O(Cl)$ with tetralin (Supporting Information Figure S17). With addition of tetralin, the absorption spectrum of $(TMP^{+\bullet})Fe^{IV}O(Cl)$ changes to $(TMP)Fe^{III}Cl$ with clear isosbestic points. The product analysis showed the formation of 1,2,3,4-tetrahydro-1-naphthol in 97% yield at 223 K and 95% yield at 193 K (Table 1). An aromatic hydroxylation product was not detected. The same product was also obtained for the reaction of $(TMP^{+\bullet})Fe^{IV}O(Cl)$ with tetralin-d_4 (Supporting Information Figure S18).

The second-order reaction rate constants (k_2) of $(TMP^{+\bullet})Fe^{IV}O(Cl)$ with tetralin and tetralin-d_4 were estimated from the dependence of the reaction rate constant (k_{obs}) on the concentration of tetralin (Table 6, and Supporting Information Figures S19−S22 and Tables S7 and S8), and the results are plotted in the Arrhenius plot (Figure 5). The Arrhenius plots

Table 6. Second-Order Reaction Rate Constants for the Reaction of $(TMP^{+\bullet})Fe^{IV}O(Cl)$ with Tetralin and Tetralin-d_4

	k_2/M^{-1} s^{-1}		
T/°C	tetralin	tetralin-d_4	KIE[a]
−40	(2.28 ± 0.01) × 10^{-1}	(8.42 ± 0.10) × 10^{-3}	27.1 (33.2)
−50	(1.17 ± 0.02) × 10^{-1}	(3.76 ± 0.03) × 10^{-3}	31.3 (39.7)
−60	(6.25 ± 0.04) × 10^{-2}	(1.58 ± 0.04) × 10^{-3}	39.7 (54.6)
−70	(3.20 ± 0.02) × 10^{-2}	(5.66 ± 0.02) × 10^{-4}	56.5 (92.8)
−80	(1.49 ± 0.02) × 10^{-2}		

[a]The numbers in parentheses are KIE values obtained after isotope purity correction with isotope purity 99.3% for tetralin-d_4.

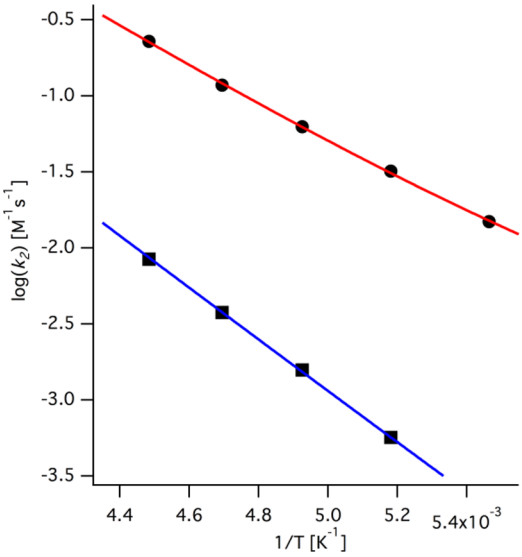

Figure 5. Arrhenius plots using second-order rate constants listed in Table 6 for the hydroxylation reactions of $(TMP^{+\bullet})Fe^{IV}O(Cl)$ with tetralin (●) and tetralin-d_4 (■). Solid lines (red line for tetralin and blue line for tetralin-d_4) are results obtained from the least-squares fits with Bell's tunneling model, eq 1. The estimated parameters are listed in Table 3.

for tetralin and tetralin-d_4 seem to show linear behavior. The Arrhenius prefactor (log A^H_{obs} = 4.7) estimated with a linear function for tetralin is smaller than that (log A^D_{obs} = 5.5) for tetralin-d_4, A^H_{obs}/A^D_{obs} = 0.16, consistent with a significant contribution of the H-tunneling process (Supporting Information Figure S6). The Arrhenius plots can be simulated well with Bell's tunneling model, eq 1. The estimated parameters are shown in Table 3.

Kinetic Isotope Effect. The hydrogen(H)/deuterium(D) primary kinetic isotope effect (KIE) is often utilized to estimate

dx.doi.org/10.1021/ic501737j | Inorg. Chem. 2014, 53, 10632−10641

the extent of involvement of the H-tunneling process in a given H-transfer reaction.[25−42] To estimate the contribution of the H-tunneling process to the present hydroxylation reactions, we calculated KIE values from the kinetic data listed in Tables 2, 4−6. The logarithms of the KIE values, $\ln(k_H/k_D)$, are plotted against $1/T$ (Figure 6). If the H(D)-transfer reaction proceeds

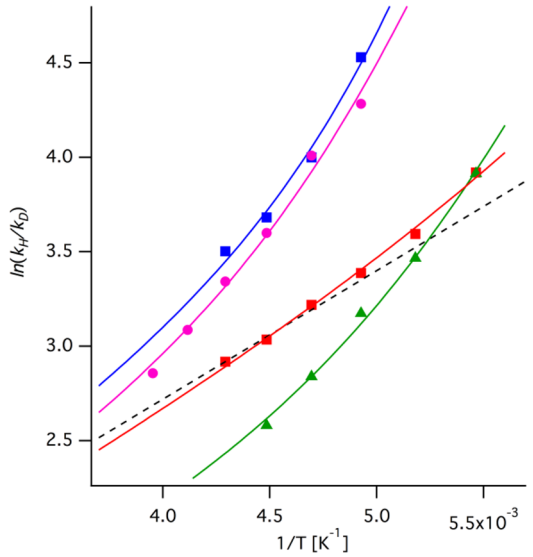

Figure 6. Plots of logarithms of KIE values after the isotope purity correction listed in Tables 2, 4−6, $\ln(k_H/k_D)$, against the reciprocal of temperature, $1/T$: pink circle, $(TMP^{+\bullet})Fe^{IV}O(NO_3)$ with xanthene; red square, $(TMP^{+\bullet})Fe^{IV}O(Cl)$ with xanthene; green triangle, $[(TMP^{+\bullet})Fe^{IV}O(Im)](NO_3)$ with xanthene; blue square $(TMP^{+\bullet})$-$Fe^{IV}O(Cl)$ with tetralin. The black broken line indicates a limit line of $\ln(k_H/k_D)$ expected from the semiclassical transition state model, $E(D) - E(H) = 5.66$ kJ/mol. Solid lines show KIE values estimated from least-squares fit with Bell's tunneling model, eq 1, and the a values obtained from the simulation of the Arrhenius plots. The estimated $E(H)$ and $E(D)$ values are listed in Table 3.

only through a transition state, without the tunneling process, the KIE values would depend solely on the difference of activation energies for H- and D-isotopomers, and the KIE value can be derived from the Arrhenius equation as

$$(k_H/k_D) = (A^H/A^D)\exp[\{E(D) - E(H)\}/RT] \quad (2)$$

where A^H and A^D are Arrhenius prefactors and $E(H)$ and $E(D)$ are activation energies for H- and D-transfer reactions, respectively. The $E(D) - E(H)$ value is determined by the zero-point energy $(h\nu/2)$ at the transition state and depends on the extent of dissociation of the C−H bond at the transition state. Previously, the maximum $E(D) - E(H)$ value can be estimated to be 5.66 kJ/mol.[43] Therefore, the $\ln(k_H/k_D)-1/T$ plot should be linear and under the maximum line (the broken line in Figure 6), and its slope should be less than the slope of the maximum line. The $\ln(k_H/k_D)-1/T$ plots for the present hydroxylation reactions either are close to or exceed these criteria. Moreover, the $\ln(k_H/k_D)-1/T$ plots are upwardly concave and can be simulated well with Bell's tunneling model. Least-square fits of the $\ln(k_H/k_D)-1/T$ plots with eq 2 also provide unusual parameters that need to consider the H-tunneling processes (Supporting Information Figure S23). The KIE plots also provide evidence of a significant contribution of the H-tunneling process to these hydroxylation reactions.

DISCUSSION

Nonlinear Arrhenius Plot. As shown in Figures 3−5, the Arrhenius plots for the hydroxylation reactions of xanthene show upward concave profiles. The observed concave profiles are not so clear, but are simulated with Bell's tunneling model better than the Arrhenius's equation (a linear function), as shown in Supporting Information Figure S7. The almost linear behavior for the D-transfer also rules out the possibility of temperature-dependent participation of other reaction pathways via different transition states and other reactive species. The results of the product analysis and product yield, as well as the presence of clear isosbestic points in the absorption spectral change, also support this conclusion. The ratios of the Arrhenius prefactors are in the range that needs to consider the H-tunneling. Thus, all of these results indicate the participation of the H-tunneling in these hydroxylation reactions. The estimated parameters from the curve fits are not sufficiently reliable to discuss the level of contribution of the H-tunneling process because the assumptions introduced in the Bell's tunneling model will lead to inaccurate results for energy ranges at the bottom and near the top of the parabolic barrier. We also analyzed the present kinetic data with Q value, which is the ratio of a tunneling correction rate and semiclassical rate (Supporting Information Figure S24). Since the Q values were sensitive to the parameters used for semiclassical rate, it was difficult to directly evaluate the level of the H-tunneling process only from the Q value. Recently, more precise two-dimensional empirical tunneling models and quantum-mechanical theories, which allow calculation of isotopic Arrhenius curves from first principles, have been developed.[57−60] Further detailed analysis of the present Arrhenius plots with these more sophisticated models will require revealing factors controlling the H-tunneling processes in their hydroxylation reactions of oxoiron(IV) porphyrin π-cation radical complexes.

KIE Value and Its Temperature Dependence. The observed KIE values and upwardly concave profiles of their temperature dependence, shown in Figure 6, clearly indicate significant contribution of the H-tunneling process in the present hydroxylation reactions. It is clear that the proportion of the H-tunneling process to the overall H-transfer reaction in the tetralin hydroxylation reaction is greater than that in the xanthene hydroxylation reaction. This result reveals that the BDE of the C−H bond is a factor controlling the proportion of the H-tunneling contribution and the proportion of the H-tunneling process in the hydroxylation reaction increases with an increase in the BDE of the C−H bond. As the BDE of the C−H bond of the substrate increases, the potential energy curve of the reactant state becomes deeper and steeper because larger energy is required to break the C−H bond. Consequently, the height of the reaction barrier becomes higher, but the thickness near the transition state becomes thinner (Supporting Information Figure S25). These changes lead to a greater H-tunneling contribution.

When we compare the KIE values in the xanthene hydroxylation reactions, the KIE value at the same temperature increases according to the order $[(TMP^{+\bullet})Fe^{IV}O(Im)](NO_3)$ < $(TMP^{+\bullet})Fe^{IV}O(Cl)$ < $(TMP^{+\bullet})Fe^{IV}O(NO_3)$, which is reverse of the reactivity order for the cyclooctene epoxidation reaction.[62] On the other hand, the slope of the line increases according to the order of $(TMP^{+\bullet})Fe^{IV}O(Cl)$ < $[(TMP^{+\bullet})$-$Fe^{IV}O(Im)](NO_3)$ < $(TMP^{+\bullet})Fe^{IV}O(NO_3)$. This order

dx.doi.org/10.1021/ic501737j | Inorg. Chem. 2014, 53, 10632−10641

correlates with the bond strengths of the Fe=O bond of these complexes estimated from resonance Raman spectroscopy: 821 cm^{-1} for $(TMP^{+\bullet})Fe^{IV}O(NO_3)$, 812 cm^{-1} for $[(TMP^{+\bullet})Fe^{IV}O(Im)](ClO_4)$, and 801 cm^{-1} for $(TMP^{+\bullet})Fe^{IV}O(Cl)$.[66−68] Since the KIE value can be changed drastically by the actual $E(D) - E(H)$ value and the height and thickness of the reaction barrier (Supporting Information Figure S26 and S27), the direct comparison of the H-tunneling contribution in three reactions may be difficult. Although further study will be needed to conclude, the reactivity of oxoiron(IV) porphyrin π-cation radical complex and the Fe=O bond strength may be factors controlling the proportion of the H-tunneling process.

It has been reported that the reactivity of oxoiron(IV) porphyrin π-cation radical complex is modulated by the nature of the porphyrin and axial ligand. The electron deficient porphyrin ligand having strong electron-withdrawing substituent has been known to increase the reactivity of oxoiron(IV) porphyrin π-cation radical complex.[23a] On the other hand, the axial ligand binding strongly to iron(III) porphyrin complex also increases the reactivity of oxoiron(IV) porphyrin π-cation radical complex.[66] Since the change of the reactivity means the change of the activation energy and the reaction free energy, the shape of the reaction barrier must be changed by the change of the reactivity. The change of the reactivity of oxoiron(IV) porphyrin π-cation radical complex would shift the potential energy curve of the reactant state upward or downward. The shift of the potential energy curve results in the change of the shape of the reaction barrier, leading to the change in the contribution of the H-tunneling process. For example, with an increase in the reactivity of oxoiron(IV) porphyrin π-cation radical complex, the potential energy curve of the reactant state shifts upward, and the reaction barrier of the hydroxylation reaction becomes lower and thicker (Supporting Information Figure S25), leading to a lesser H-tunneling contribution. Previously, the KIE value of cyclohexane hydroxylation reaction was reported to become lower with an increase in the electron-withdrawing effect of the meso-substituent.[31] Although the reported KIE values are not so high as to expect large H-tunneling contribution, this observation can be interpreted by the change of the H-tunneling contribution as discussed here.

The Fe=O bond strength would not modulate the shape of the potential energy curve because the shape (curvature) of the potential energy surface of the reactant state for the hydroxylation reaction is mainly determined by the nature of the C—H bond of substrate. Furthermore, since our previous report concluded that the Fe=O bond strength of oxoiron(IV) porphyrin π-cation radical complex does not correlate with its reactivity,[63] the Fe=O bond strength does not control the H-tunneling process with shifting the potential energy curve upward or downward, as proposed for the reactivity change. It is difficult to explain the correlation between the Fe=O bond strength and the H-tunneling process with the change of the reactant state. A possible explanation is that the Fe=O bond strength correlates with the FeO—H bond strength of iron(IV)-hydroxide intermediate, which is produced after the H-transfer reaction (the product state of the H-transfer reaction). The FeO—H bond strength changes the shape of the potential energy curve of a product state. Thus, it also changes the shape of the reaction barrier of the H-transfer reaction, leading to the change of the H-tunneling process. As discussed in the paragraph above, since the H-transfer reaction to an oxoiron(IV) porphyrin π-cation radical complex having weak Fe=O bond expects to produce an iron(IV)-hydroxide complex having weak FeO—H bond, the reaction barrier of the H-transfer reaction would be thicker, and thus the H-tunneling contribution would be smaller, as the Fe=O bond becomes weaker.

Finally, it is clear from Figure 6 that the reaction temperature is an important factor to determine the H-tunneling contribution. This phenomenon has been reported for decades.[43−61] With a decrease in the reaction temperature, the reaction occurring via the transition state contributes to a lesser degree than the reaction occurring via the H-tunneling process because the H-tunneling occurs at lower energy barrier. Thus, the H-tunneling contribution increases as the reaction temperature decreases. As previous reports pointed out, we point out here again that caution should be taken with respect to a measured temperature when the KIE values are being compared.

In summary, we have performed a kinetic study of hydroxylation reactions at the benzylic positions of xanthene and tetralin with $(TMP^{+\bullet})Fe^{IV}O(L)$ under single-turnover conditions to investigate the factors controlling the H-tunneling process and succeeded in the observation of nonlinear Arrhenius plots. The analysis performed in this study indicates that the extent of the H-tunneling contribution is controlled by the BDE of the C—H bond of the substrate, the reactivity of oxoiron(IV) porphyrin π-cation radical, and probably the Fe=O bond strength.

EXPERIMENTAL SECTION

Instruments. UV−vis absorption spectra were recorded on an Agilent 8453 spectrophotometer (Agilent Technologies) equipped with USP-203 low-temperature chamber (UNISOKU). Gas chromatography−mass spectrometry (GC−MS) analysis was performed on a QP-5000 GC−MS system (Shimadzu) equipped with a capillary gas chromatograph (GC-17A, CBP5-M25-025 capillary column). ^1H NMR spectra were measured on a Lambda-500 spectrometer (JEOL). ^1H NMR chemical shifts were recorded versus tetramethylsilane (TMS) and referenced to a residual solvent peak, dichloromethane 5.32 ppm and chloroform 7.23 ppm. Ozone gas was generated by UV irradiation of oxygen gas (99.9%) with an ozone generator PR-1300 (ClearWater) and used without further purification.

Materials. Anhydrous dichloromethane was purchased from Kanto and was stored in the presence of 4 Å molecular sieves. The other anhydrous and spectrophotometric grade solvents were commercially obtained and were used as received. Xanthene and xanthydrol were purchased from Sigma-Aldrich. 1,2,3,4-Tetrahydronaphthalene (tetralin) was purchased from Tokyo Kasei, and 1,2,3,4-tetrahydro-1-naphthol was purchased from Wako. Chloroform-d_1, dichloromethane-d_2, deuterium oxide (D_2O), and dimethyl sulfoxide-d_6 (DMSO-d_6) were purchased from Cambridge Isotope Laboratories Inc. Sodium hydride (55% dispersion in mineral oil) was purchased from Wako and purified by washing with hexane just before use. Undecane was purchased from Kanto. To remove a trace of impurity, xanthene dissolved in small amount of dichloromethane and neat tetralin was passed through activated alumina just before use. The concentration of xanthene solution after the purification was determined for each preparation by the absorbance at 249 nm, $\varepsilon_{249\ nm} = 7872.4\ M^{-1}\ cm^{-1}$ in dichloromethane at room temperature. 5,10,15,20-Tetramesitylporphyrin ($TMPH_2$) was prepared according to the process described in the literature.[69] $(TMP)Fe^{III}Cl$ was prepared by the reaction of $TMPH_2$ with $FeCl_2$ and sodium acetate in acetic acid and purified by silica gel column chromatography using CH_2Cl_2/CH_3OH as an eluent.[62] $(TMP)Fe^{III}NO_3$ was prepared by the reaction of $(TMP)Fe^{III}Cl$ with silver nitrate in tetrahydrofuran at room temperature and purified by recrystallization from dichloromethane/*n*-hexane.[70]

dx.doi.org/10.1021/ic501737j | Inorg. Chem. 2014, 53, 10632−10641

Xanthene-d_2 was prepared according to the procedure described in the literature.[71] A mixture of xanthene (1 g, 5.5 mmol) and DMSO-d_6 (D: 99.9%, 6 mL) together with sodium hydride (0.4 g, 16.7 mmol) under an inert (argon) atmosphere was stirred at room temperature overnight. The reaction was quenched with 10 mL of D_2O (D: 99.9%). The crude product was filtered and washed with a large volume of water. The product was purified by recrystallization from ethanol. ^{1}H NMR spectra confirmed about 99% deuterium incorporation. The same procedure was repeated with DMSO-d_6 (D: 99.96%, 6 mL). The deuterated xanthene-d_2 was further purified by passing through activated alumina just before use. The purified xanthene-d_2 showed about 99.8 atom % deuteration (Supporting Information Figure S28). The xanthene-d_2 solution was also passed through activated alumina just before use, and the concentration for each preparation was determined from the absorbance at 249 nm.

1,2,3,4-Tetrahydronaphthalene-d_4 (tetralin-d_4) was prepared using a similar method.[72] A mixture of sodium hydride (0.72 g, 30 mmol) and DMSO-d_6 (D: 99.9%, 11.55 mL) was stirred for 30 min at room temperature under an inert (argon) atmosphere. Then, tetralin (1.00 g, 7.58 mmol) was added to the solution, and the mixture was stirred at room temperature for more than 48 h. The reaction was quenched with D_2O (D: 99.9%, 10 mL). Hexane (30 mL) was added, and the mixture was separated. The organic phase was extracted by hexane (30 × 2 mL) and then washed with water (40 × 2 mL). The solution was dried with anhydrous sodium sulfate, and the solvent was removed under reduced pressure to give the crude tetralin-d_4. The product was purified vacuum distillation. To improve the isotope purity, this procedure was repeated three times. The final product was further purified by passing it through a silica gel column using hexane as the eluent. ^{1}H NMR spectra of the purified tetralin-d_4 showed about 99.3 atom % deuterium incorporation (Supporting Information Figure S29). The tetralin-d_4 was also passed through activated alumina just before use.

Kinetic Analysis. Iron(III) porphyrin complex ((TMP)$Fe^{III}NO_3$ or (TMP)$Fe^{III}Cl$, 1.0×10^{-4} M) dissolved in dichloromethane in a 1 cm quartz cuvette was placed in a low-temperature chamber set in a UV−vis absorption spectrometer. After cooling the sample solution to a desired temperature (−20 to −95 °C), ozone gas was passed through the solution using a gastight syringe. The formation of oxoiron(IV) porphyrin π-cation radical complex, ($TMP^{+\bullet}$)$Fe^{IV}O(NO_3)$ or ($TMP^{+\bullet}$)$Fe^{IV}O(Cl)$, was monitored by the absorption spectroscopy. [($TMP^{+\bullet}$)$Fe^{IV}O(Im)$](NO_3) was prepared by the addition of 1 equiv of imidazole (1.0×10^{-4} M) to ($TMP^{+\bullet}$)$Fe^{IV}O(NO_3)$. The remaining ozone was removed by bubbling dry argon gas with a gastight syringe (~10 mL). Xanthene or tetralin dissolved in dichloromethane was added to the sample solution with stirring. The reaction was monitored by observing the absorption spectral change at a constant time interval immediately after addition. The pseudo-first-order rate constant (k_{obs}) was determined by the least-squares fit of the time-course of the absorbance at 668 nm for ($TMP^{+\bullet}$)$Fe^{IV}O(NO_3)$ and [($TMP^{+\bullet}$)$Fe^{IV}O(Im)$](NO_3), and at 667 nm for ($TMP^{+\bullet}$)$Fe^{IV}O(Cl)$ with single-exponential function by a curve-fitting program in Igor (WaveMetrics, Inc.). The pseudo-first-order rate constant was found to be linearly dependent upon the concentration of substrate. The second-order rate constant (k_2) was determined by a least-squares fit of the dependence with the following equation, $k_{obs} = k_0 + k_2$[substrate], where k_0 is the rate constant for the self-decomposition of the oxoiron(IV) porphyrin π-cation radical complex.

Since the observed reaction rate constant for deuterated sample is the sum of reaction rate constants for the D-transfer reaction and the unlabeled H-transfer reaction, the second-order rate constant for 100% pure deuterated sample, k_D(correction), was calculated with the following equation, eq 3

$$k_D(\text{correction}) = \{k_D - k_H \times (1 - \text{DP}/100)\} \times 100/\text{DP} \quad (3)$$

where k_H and k_D are the second-order reaction rate constants obtained from experiments for H- and D-isotopomers, respectively, and DP is the deuterium isotope purity (%). The KIE value obtained after the isotope purity correction was calculated with k_D(correction), KIE-(correction) = k_H/k_D(correction).

The least-squares curve fits with the Bell's tunneling model, eq 1, require estimation of three parameters, the Arrhenius prefactor (A), thickness of the reaction barrier (a), and the activation energy (E), for one kinetic data set. There are many combinations of these parameters that can simulate well the experimental Arrhenius plot. Although Bell's tunneling model expects E(D) − E(H) less than 5.66 kJ/mol and very similar A and a values between H- and D-isotopomers, we could not obtain reliable parameters satisfying these conditions from the least-squares curve fit with eq 1 without any restrictions. Therefore, we first roughly estimated the A value from Arrhenius plot for D-isotopomer with a linear function, and then repeated least-squares fit of the Arrhenius plot for H-isotopomer with eq 1 to be better fit by adjusting the estimated A value, allowing determination of the A, a, and E(H) values. Finally, the E(D) value is determined by least-squares curve fit of the Arrhenius plot for D-isotopomer with eq 1 including the A and a values determined from the curve fit of H-isotopomer.

Product Analysis. For xanthene hydroxylation, oxoiron(IV) porphyrin π-cation radical complex (1.0×10^{-3} M) was prepared in dichloromethane-d_2 in a two-neck Schlenk tube using the same method described above. Xanthene (2−20 equiv) was added to the sample solution at the same temperature. The solution was stirred until the green solution changed to reddish (over the course of several minutes). After being warmed to room temperature, the sample solution was transferred to a 5 mm NMR tube, and the ^{1}H NMR spectrum was measured at 25 °C. The product was assigned on the basis of ^{1}H NMR chemical shifts of xanthydrol and xanthenone. The yield of the product (xanthydrol) was determined by the percentage of the peak area over the iron porphyrin signals. The same experiment was repeated three times, and the product yields were determined from the average of three experiments.

For tetralin hydroxylation, oxoiron(IV) porphyrin π-cation radical complex (5.0×10^{-4} M) was prepared in a two-neck Schlenk tube using the same method described in the above section. Tetralin (0.1−0.6 M) was added to the sample solution at the same temperature. The solution was stirred until the green solution changed to reddish (over the course of several minutes). After warming to room temperature, the products were analyzed by GC−MS. 1,2,3,4-Tetrahydro-1-naphthol was an only product, and other products including aromatic hydroxylation products were not detected. The yield of 1,2,3,4-tetrahydro-1-naphthol was determined by GC−MS with a calibration line using undecane as an internal standard. The same experiment was repeated three times, and the product yields were determined from the average of three experiments.

■ ASSOCIATED CONTENT

Ⓢ Supporting Information

Figures S1 to S28 and Tables S1 to S8. This material is available free of charge via the Internet at http://pubs.acs.org.

■ AUTHOR INFORMATION

Corresponding Author

*E-mail: fujii@cc.nara-wu.ac.jp.

Notes

The authors declare no competing financial interest.

■ ACKNOWLEDGMENTS

We thank Professor Masahiko Hada (Tokyo Metropolitan University), Professor Kenichi Kinugawa (Nara Women's University), and Dr. Minoru Kubo (RIKEN) for many helpful discussions and comments. This work was supported by grants from JSPS (Grants-in-Aid for Scientific Research, Grant 25288032).

■ REFERENCES

(1) Sono, M.; Roach, M. P.; Coulter, E. D.; Dawson, J. H. *Chem. Rev.* **1996**, *96*, 2841−2887.

(2) Costas, M.; Chen, K.; Que, L., Jr. *Coord. Chem. Rev.* **2000**, *200*−*202*, 517−544.
(3) Groves, J. T. *J. Inorg. Biochem.* **2006**, *100*, 434−447.
(4) Oritz de Montellano, P. R. *Chem. Rev.* **2010**, *110*, 932−948.
(5) Baik, M.-H.; Newcomb, M.; Friesner, R. A.; Lippard, S. J. *Chem. Rev.* **2003**, *103*, 2385−2419.
(6) Che, C.-M.; Lo, V. K.-Y.; Zhou, C.-Y.; Huang, J.-S. *Chem. Soc. Rev.* **2011**, *40*, 1950−1975.
(7) (a) Periana, R. A.; Taube, D. J.; Gamble, S.; Taube, H.; Satoh, T.; Fujii, H. *Science* **1998**, *280*, 560−564. (b) Conley, B. L.; Tenn, W. J., III; Young, K. J. H.; Ganesh, S. K.; Meier, S. K.; Ziatdinov, V. R.; Mironov, O.; Oxgaard, J.; Gonzales, J.; Goddard, W. A., III; Periana, R. A. *J. Mol. Catal. A: Chem.* **2006**, *251*, 8−23.
(8) (a) Das, S.; Incarvito, C. D.; Crabtree, R. H.; Brudvig, G. W. *Science* **2006**, *312*, 1941−1943. (b) Chen, M. S.; White, M. C. *Science* **2007**, *318*, 783−786. (c) Kamata, K.; Yonehara, K.; Nakagawa, Y.; Uehara, K.; Mizuno, N. *Nat. Chem.* **2010**, *2*, 478−483. (d) Chen, M. S.; White, M. C. *Science* **2010**, *327*, 566−571. (e) Kojima, T.; Nakayama, K.; Ikemura, K.; Ogura, T.; Fukuzumi, S. *J. Am. Chem. Soc.* **2011**, *133*, 11692−11700. (f) Seo, M. S.; Kim, N. H.; Cho, K.-B.; So, J. E.; Park, S. K.; Clémancey, M.; Garcia-Serres, R.; Latour, J.-M.; Shaik, S.; Nam, W. *Chem. Sci.* **2011**, *2*, 1039−1045. (g) Hitomi, Y.; Arakawa, K.; Funabiki, T.; Kodera, M. *Angew. Chem., Int. Ed.* **2012**, *51*, 3448−3452. (h) Wilson, A. A.; Chen, J.; Hong, S.; Lee, Y.-M.; Clémancy, M.; Garcia-Serres, R.; Nomura, T.; Ogura, T.; Latour, J.-M.; Hedman, B.; Hodgson, K. O.; Nam, W.; Solomon, E. I. *J. Am. Chem. Soc.* **2012**, *134*, 11791−11806.
(9) Kudrik, E. V.; Afanasiev, P.; Alvarez, L. X.; Dubourdeaux, P.; Clémancey, M.; Latour, J.-M.; Blondin, G.; Bouchu, D.; Albrieux, F.; Nefedov, S. E.; Sorokin, A. B. *Nat. Chem.* **2012**, *4*, 1024−1029.
(10) Denisov, I. G.; Makris, T. M.; Sligar, S. G.; Schlichting, I. *Chem. Rev.* **2005**, *105*, 2253−2278.
(11) (a) Kandel, S.; Sauveplane, V.; Olry, A.; Diss, L.; Benveniste, I.; Pinot, F. *Phytochem. Rev.* **2006**, *5*, 359−372. (b) Van Bogaert, I. N. A.; Groeneboer, S.; Saerens, K.; Soetaert, W. *FEBS J.* **2011**, *278*, 206−221.
(12) (a) Groves, J. T.; Nemo, T. E.; Myers, R. S. *J. Am. Chem. Soc.* **1979**, *101*, 1032−1033. (b) Groves, J. T.; Nemo, T. E. *J. Am. Chem. Soc.* **1983**, *105*, 6243−6248.
(13) Meunier, B. *Chem. Rev.* **1992**, *92*, 1411−1456.
(14) Dolphin, D.; Traylor, T. G.; Xie, L. Y. *Acc. Chem. Res.* **1997**, *30*, 251−259.
(15) (a) Bartoli, J. F.; Battioni, P.; De Foor, W. R.; Mansuy, D. *J. Chem. Soc., Chem. Commun.* **1994**, 23−24. (b) Bartoli, J. F.; Brigaud, O.; Battioni, P.; Mansuy, D. *J. Chem. Soc., Chem. Commun.* **1991**, 440−442.
(16) Higuchi, T.; Uzu, S.; Hirobe, M. *J. Am. Chem. Soc.* **1990**, *112*, 7051−7052.
(17) Lu, H.; Zhang, P. *Chem. Soc. Rev.* **2011**, *40*, 1899−1909.
(18) Rittle, J.; Green, M. T. *Science* **2010**, *330*, 933−937.
(19) Wang, X.; Peter, S.; Kinne, M.; Hofrichter, M.; Groves, J. T. *J. Am. Chem. Soc.* **2012**, *134*, 12897−12900.
(20) Davydov, R.; Gilep, A. A.; Stushkevich, N. V.; Usanov, S. A.; Hoffman, B. M. *J. Am. Chem. Soc.* **2012**, *134*, 17149−17156.
(21) Schlichting, I.; Berendzen, J.; Chu, K.; Stock, A. M.; Maves, S. A.; Benson, D. E.; Sweet, R. M.; Ringe, D.; Petsko, G. A.; Sligar, S. G. *Science* **2000**, *287*, 1615−1622.
(22) Groves, J. T.; Haushalter, R. C.; Nakamura, M.; Nemo, T. E.; Evans, B. J. *J. Am. Chem. Soc.* **1981**, *103*, 2884−2886.
(23) (a) Fujii, H. *J. Am. Chem. Soc.* **1993**, *115*, 4641−4648. (b) Watanabe, Y.; Fujii, H. In *Metal-Oxo and Metal-Peroxo Species in Catalytic Oxidations*; Meunier, B., Ed.; Springer: New York, 2000; Vol. *97*, pp 61−89. (c) Fujii, H. *Coord. Chem. Rev.* **2002**, *226*, 51−60.
(24) Groves, J. T.; McClusky, G. A. *J. Am. Chem. Soc.* **1976**, *98*, 859−861.
(25) Hjelmeland, L. M.; Aronow, L.; Trudell, J. R. *Biochem. Biophys. Res. Commun.* **1977**, *76*, 541−549.
(26) (a) Nelson, S. D.; Trager, W. F. *Drug Metab. Dispos.* **2003**, *31*, 1481−1498. (b) Jones, J. P.; Trager, W. F. *J. Am. Chem. Soc.* **1987**, *109*, 2171−2173.
(27) Kadkhodayan, S.; Coulter, E. D.; Maryniak, D. M.; Bryson, T. A.; Dawson, J. H. *J. Biol. Chem.* **1995**, *270*, 28042−28048.
(28) Lindsay Smith, J. R.; Piggott, R. E.; Sleath, P. R. *J. Chem. Soc., Chem. Commun.* **1982**, 55−56.
(29) Sorokin, A. B.; Khenkin, A. M. *J. Chem. Soc., Chem. Commun.* **1990**, 45−46.
(30) Sorokin, A. B.; Robert, A.; Meunier, B. *J. Am. Chem. Soc.* **1993**, *115*, 7293−7299.
(31) Lim, M. H.; Lee, Y. J.; Goh, Y. M.; Nam, W.; Kim, C. *Bull. Chem. Soc. Jpn.* **1999**, *72*, 707−713.
(32) Pan, Z.; Horner, J. H.; Newcomb, M. *J. Am. Chem. Soc.* **2008**, *130*, 7776−7777.
(33) Jonsson, T.; Glickman, M. H.; Sun, S. J.; Klinman, J. P. *J. Am. Chem. Soc.* **1996**, *118*, 10319−10320.
(34) Glickman, M. H.; Wiseman, J. S.; Klinman, J. P. *J. Am. Chem. Soc.* **1994**, *116*, 793−794.
(35) Ambundo, E. A.; Friesner, R. A.; Lippard, S. J. *J. Am. Chem. Soc.* **2002**, *124*, 8770−8771.
(36) (a) Panay, A. J.; Lee, M.; Krebs, C.; Bollinger, J. M., Jr.; Fitzpatrick, P. F. *Biochemistry* **2011**, *50*, 1928−1933. (b) Panay, A. J.; Fitzpatrick, P. F. *Biochemistry* **2008**, *47*, 11118−11124.
(37) Pavon, J. A.; Fitzpatrick, P. F. *J. Am. Chem. Soc.* **2005**, *127*, 16414−16415.
(38) Hoffart, L. M.; Barr, E. W.; Guyer, R. B.; Bollinger, J. M., Jr.; Krebs, C. *Proc. Natl. Acad. Sci. U.S.A.* **2006**, *103*, 14738−14743.
(39) Price, J. C.; Barr, E. W.; Glass, T. E.; Krebs, C.; Bollinger, J. M., Jr. *J. Am. Chem. Soc.* **2003**, *125*, 13008−13009.
(40) Nesheim, J.; Lipscomb, J. D. *Biochemistry* **1996**, *35*, 10240−10247.
(41) Kaizer, J.; Kinker, E. J.; Oh, N. Y.; Rohde, J.-U.; Song, W. J.; Stubna, A.; Kim, J.; Münck, E.; Nam, W.; Que, L., Jr. *J. Am. Chem. Soc.* **2004**, *126*, 472−473.
(42) (a) Mahapatra, S.; Halfen, J. A.; Tolman, W. B. *J. Am. Chem. Soc.* **1996**, *118*, 11575−11586. (b) Park, K.; Pak, Y.; Kim, Y. *J. Am. Chem. Soc.* **2012**, *134*, 3524−3531.
(43) Bell, R. P. *The Tunnel Effect in Chemistry*; Chapman and Hall: London, 1980.
(44) Caldin, E. F. *Chem. Rev.* **1969**, *69*, 135−156.
(45) (a) Klinman, J. P. *Biochemistry* **2013**, *52*, 2068−2077. (b) Nagel, Z. D.; Klinman, J. P. *Chem. Rev.* **2006**, *106*, 3095−3118. (c) Klinman, J. P. *Biochim. Biophys. Acta* **2006**, *1757*, 981−987. (d) Bahnson, B. J.; Klinman, J. P. *Methods Enzymol.* **1995**, *249*, 375−397.
(46) (a) Sen, A.; Kohen, A. *J. Phys. Org. Chem.* **2010**, *23*, 613−619. (b) Kohen, A. In *Isotope Effects in Chemistry and Biology*; Kohen, A., Limbach, H.-H., Eds.; Taylor and Francis: New York, 2006; pp 743−764. (c) Kohen, A.; Klinman, J. P. *Chem. Biol.* **1999**, *6*, R191−R198. (d) Kohen, A.; Klinman, J. P. *Acc. Chem. Res.* **1998**, *31*, 397−404.
(47) Marcus, R. A. *Philos. Trans. R. Soc., B* **2006**, *361*, 1445−1455.
(48) O'Ferrall, R. A. M. *J. Phys. Org. Chem.* **2010**, *23*, 572−579.
(49) Kamerlin, S. C. L.; Warshel, A. *J. Phys. Org. Chem.* **2010**, *23*, 677−684.
(50) (a) Limbach, H.-H.; Schowen, K. B.; Schowen, R. L. *J. Phys. Org. Chem.* **2010**, *23*, 586−605. (b) Limbach, H.-H.; Lopez, J. M.; Kohen, A. *Philos. Trans. R. Soc., B* **2006**, *361*, 1399−1415.
(51) Bothma, J. P.; Gilmore, J. B.; McKenzie, R. H. *New J. Phys.* **2010**, *12*, 055002.
(52) (a) Bell, R. P. *Proc. R. Soc. London, Ser. A* **1935**, *148*, 241−250. (b) Eckart, C. *Phys. Rev.* **1930**, *35*, 1303−1309.
(53) Bruniche-Olsen, N.; Ulstrup, J. *J. Chem. Soc., Faraday Trans. 1* **1979**, *75*, 205−226.
(54) German, E. D.; Kuznetsov, A. M.; Dogonadze, R. R. *J. Chem. Soc., Faraday Trans. 1* **1980**, *76*, 1128−1146.
(55) Kuznetsov, A. M.; Ulstrup, J. In *Isotope Effects in Chemistry and Biology*; Kohen, A., Limbach, H.-H., Eds.; Taylor and Francis: New York, 2006; pp 691−724.
(56) (a) Siebrand, W.; Wildman, T. A.; Zgierski, M. Z. *J. Am. Chem. Soc.* **1984**, *106*, 4083−4089. (b) Siebrand, W.; Wildman, T. A.; Zgierski, M. Z. *J. Am. Chem. Soc.* **1984**, *106*, 4089−4096.
(57) Truhlar, D. G. *J. Phys. Org. Chem.* **2010**, *23*, 660−676.

(58) Siebrand, W.; Smedarchina, Z. *J. Phys. Chem. B* **2011**, *115*, 7679−7692.
(59) Brackhagen, O.; Scheurer, Ch.; Meyer, R.; Limbach, H.-H. *Ber. Bunsen-Ges.* **1998**, *102*, 303−316.
(60) (a) Antoniou, D.; Schwartz, S. D. *J. Phys. Chem. B* **2001**, *105*, 5553−5558. (b) Antoniou, D.; Schwartz, S. D. *Proc. Natl. Acad. Sci. U.S.A.* **1997**, *94*, 12360−12365.
(61) Layfield, J. P.; Hammes-Schiffer, S. *Chem. Rev.* **2013**, *114*, 3466−3494.
(62) Takahashi, A.; Kurahashi, T.; Fujii, H. *Inorg. Chem.* **2009**, *48*, 2614−2625.
(63) Luo, Y.-R. *Handbook of Bond Dissociation Energies in Organic Compounds*; CRC Press: New York, 2003.
(64) Bell, S. R.; Groves, J. T. *J. Am. Chem. Soc.* **2009**, *131*, 9640−9641.
(65) (a) Shaik, S.; Kumar, D.; de Visser, S. P.; Altun, A.; Thiel, W. *Chem. Rev.* **2005**, *105*, 2279−2328. (b) Shaik, S.; Lai, W.; Chen, H.; Wang, Y. *Acc. Chem. Res.* **2010**, *43*, 1154−1165.
(66) Takahashi, A.; Yamaki, D.; Ikemura, K.; Kurahashi, T.; Ogura, M.; Hada, H.; Fujii, H. *Inorg. Chem.* **2012**, *51*, 7296−7305.
(67) Czarnecki, K.; Kincaid, J. R.; Fujii, H. *J. Am. Chem. Soc.* **1999**, *121*, 7953−7954.
(68) Czarnecki, K.; Nimri, S.; Gross, Z.; Proniewicz, L. M.; Kincaid, J. R. *J. Am. Chem. Soc.* **1996**, *118*, 2929−2935.
(69) Lindsey, J.; Wagner, R. *J. Org. Chem.* **1989**, *54*, 828−836.
(70) Wyllie, G. R. A.; Munro, O. Q.; Schulz, C. E.; Scheidt, W. R. *Polyhedron* **2007**, *26*, 4664−4672.
(71) Sastri, C. V.; Lee, J.; Oh, K.; Lee, Y. J.; Lee, J.; Jackson, T. A.; Ray, K.; Hirao, H.; Shin, W.; Halfen, J. A.; Kim, J.; Que, L., Jr.; Shaik, S.; Nam, W. *Proc. Natl. Acad. Sci. U.S.A.* **2007**, *104*, 19181−19186.
(72) Comita, P. B.; Berman, M. R.; Moore, C. B.; Bergman, R. G. *J. Phys. Chem.* **1981**, *85*, 3266−3276.